TRACKLET-BASED CORRELATION OF COMBINED RADAR AND OPTICAL MEASUREMENTS

Benedikt Reihs, Alessandro Vananti, and Thomas Schildknecht

Astronomical Institute University of Bern (AIUB), Sidlerstrasse 5, 3012 Bern, Switzerland
Email: benedikt.reihs@aiub.unibe.ch

ABSTRACT

The ongoing growth of the space debris population leads to an increasing importance of space surveillance tasks to build and maintain knowledge about the object densities in different Earth orbits. Due to numerous fragmentation events, also the highly elliptical orbits contain increasing amounts of space debris. For standard survey measurements, objects in these orbits are either detected by radar close to their perigee or by telescopes close to their apogee. Usually, one single sequence of measurements, called tracklet, is too short to obtain a reliable orbit and instead two tracklets are combined to test if they originate from the same object. This process is called correlation. If radar and optical measurements are treated separately, only limited information about the orbit is available. To improve the processing of these objects, this paper proposes a method for the correlation and initial orbit determination by combining radar and optical tracklets. The method is based on a previously developed radar-only method, which also includes corrections of the J_2-perturbations. Simulated survey measurements are used to test the new method and compare it to the radar-only case. It is shown that the radar-optical correlation achieves satisfying results. It also matches the measurements better and gives more precise orbits compared to the radar-only approach.

Keywords: radar; optical; data fusion; tracklet correlation.

1. INTRODUCTION

The continuous growth of the space debris population is an increasing risk for operational satellites and the long-term sustainability of orbits around Earth. Apart from the typically mentioned regions in the low earth orbit (LEO) and the geostationary orbit (GEO), the highly eccentric orbits (HEO), e.g. the geotransfer orbit (GTO), also show increasing space debris populations, mainly due to breakup events [1]. As the HEO objects pass through LEO and potentially also close to GEO, they pose a potential collision risk for objects in both these important regions and may even couple the overall collision risk for objects in these distant orbits [8]. In order to mitigate this risk at least for conjunctions involving active satellites, the orbits of HEO objects have to be maintained with the help of regular observations. One problem is that if these objects are only observed by standard radar or optical measurements, the detections are all around perigee or apogee, respectively. This would severely limit the information available and increase the uncertainties of the calculated orbits. Thus it is expected that a combined processing of radar and optical measurements improves the quality of the orbit solution. While the routine update of an orbit stored in a database can be done involving different measurement types, the treatment of detections which cannot be assigned to a known object is more challenging.

The sequence of measurements from a single pass, called tracklet, is often too short to produce a reliable result via a classical orbit determination. In such a case two tracklets are combined and an orbit is derived from their merged data to test if they originate from the same object. This process is called correlation. Various methods for the correlation of these short tracklets have been developed for different measurement types. For the correlation of optical tracklets, different approaches exist, see e.g. [2, 4, 12], as well as methods for the correlation of radar measurements, see e.g. [6, 11]. A method for the radar-optical case, which is the focus of this paper, has been proposed by [5] in the measurement space using the approach of the integrals of motion and by [14] in the orbit space performing an initial orbit determination with the radar tracklet.

In the following, a method for the direct correlation of radar and optical measurements based on a boundary value problem is proposed focussing on the case of objects in HEO. It was shown previously [11] that the radar-only correlation of HEO objects has more difficulties and errors than the LEO case, which is the main motivation to extend it to optical measurements and check for an additional benefit.

2. CORRELATION METHOD

2.1. Theory

The authors of this paper previously proposed a method for the correlation of radar tracklets, see [11], based on a two positions boundary value problem including correction of the J_2-perturbation. This method is extended in this work to combine tracklets measured by radar and optical systems already during the initial orbit determination and correlation process.

The measurements are processed as attributables [9], which is a virtual measurement obtained by fitting the measurements to a function over time, thus condensing the information in the tracklet to reduce the influence of noise. By combining one optical and one radar tracklet the attributable vectors are:

$$\mathscr{A}_r = \{t_r, \rho_r, \dot{\rho}_r, az, el\}\,, \quad (1)$$

$$\mathscr{A}_o = \{t_o, \alpha, \delta, \dot{\alpha}, \dot{\delta}\}\,, \quad (2)$$

containing the radar measurements: range ρ_r, range-rate $\dot{\rho}_r$, azimuth az, elevation el, and the optical measurements: right ascension α, declination δ and their time-derivatives $\dot{\alpha}, \dot{\delta}$. Both are given at their respective times t_r and t_o. The attributable could also be extended to contain further information, e.g. the location of the observer, but this is left out here due to simplicity.

In order to apply the boundary positions method, it is necessary to add a hypothesis on the range ρ_o at the time of the optical measurement t_o. This is also an improvement compared to the correlation of two optical tracklets, which requires two hypotheses [12]. The range hypothesis is combined with the range and angular measurements to compute the orbit between the two positions.

$$\begin{array}{ccc} \{\rho_o\} & \rightarrow & \text{Hypothesis} \\ \{\rho_r, az, el, \rho_o, \alpha, \delta\} & \rightarrow & \text{Orbit} \\ \{\dot{\rho}_r, \dot{\alpha}, \dot{\delta}\} & \rightarrow & \text{Discriminator} \end{array}$$

The remaining measurements form the so-called discriminator $\vec{x}$. In the discriminator, the measured elements $\vec{x}_m$ are compared to the elements $\vec{x}_c$ computed from the derived orbit. The difference between them, $\Delta\vec{x}$, is related to their covariance matrix $C_{m,c}$ to give the Mahalanobis distance M_d [7]:

$$M_d = \sqrt{\Delta\vec{x}^T \cdot C_{m,c}^{-1} \cdot \Delta\vec{x}}. \quad (3)$$

The Mahalanobis distance is a statistical distance measure which scales the difference by its uncertainty and thus yields a normalised distance measure. Together with a threshold value $M_{d,thresh}$, the two tracklets are considered to be correlated if $M_d < M_{d,thresh}$.

The covariance matrix $C_{m,c} = C_m + C_c$ is the sum of the covariance due to the measurements C_m, derived via the attributable fit, and the uncertainty due to the initial orbit C_c, which is a mapping of the parameters' measurement uncertainty used for the orbit computation onto the discriminator vector. The influence of these contributions will be analysed later.

In practice, the correlation leads to an optimisation problem of finding the best hypothesis on the optical range, i.e. the one which results in the lowest Mahalanobis distance. A search along ρ_o is performed using a line search with a numerical gradient approximation to find the minimum of M_d. Once a value for the range ρ_o is set, two positions are available and thus the orbit determination via the boundary positions method can be used. As a short summary, this method uses a variation of the iteration on the semi-parameter, p-iteration [3]. Additionally, corrective rotations of the second measurement point are performed to correct for the changes due to J_2-perturbation. One around the Earth rotation axis to correct the orbital plane and one simple summation to correct the location of the perigee. Internally, the propagation is performed with the J_2-corrected Keplerian mean motion to increase the efficiency compared to the use of numerical propagation, see [11] for more details.

2.2. Loss Function Topography

As a first step, the topography of the loss function M_d shall be analysed to test if it can be optimised easily. One example of a loss function is given in Figure 1, which also shows that another dimension of the problem has to be considered. Depending on the time between the two tracklets, the connection of the two points may be possible with different numbers of completed revolutions. In the plot, it can be seen that there is a distinct minimum for each number of revolutions with different minimum values. The absolute minimum and true solution can be found at ten revolutions in this example.

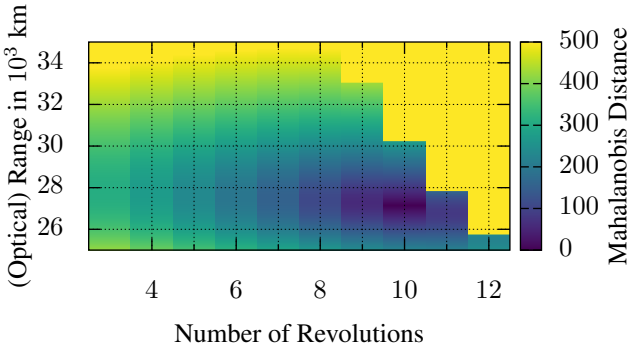

Figure 1. Example of the loss function M_d for a specific pair of tracklets.

To analyse this further, Figure 2 depicts the Mahalanobis distance over the hypothetical range for the absolute minimum from the previous plot which represents one single optimisation problem of the correlation. A distinct mini-

mum encompassed by two nearly linear slopes is visible, which should be found in an optimisation process using numerically calculated gradients. Practically, the minimum for each feasible number of revolutions has to be calculated and then the one with the lowest Mahalanobis distance is chosen as the final solution.

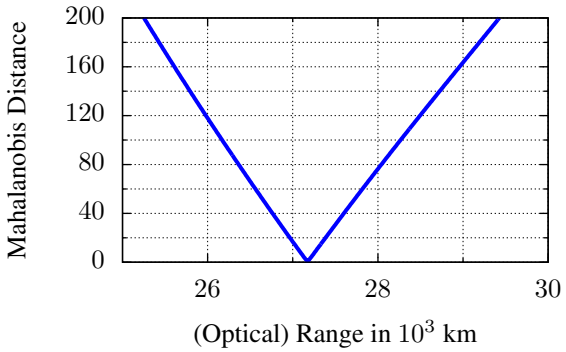

Figure 2. Example of the one-dimensional optimisation problem for one specific number of revolutions.

3. SIMULATIONS

The simulated measurements use an object population extracted from Space-Track [13] which is propagated numerically [10]. Different measurement stations and object populations in HEO are simulated with the parameters given in Table 1. Depending on the scenario, the simulations have different durations ranging from three days for a multi-station setup to eleven days for a single station in central Europe. Different scenarios are necessary because the sub-population which can be observed at perigee by a radar and close to apogee by a telescope at night-time is limited. In order to obtain a larger sample, the results from the different radar-optical surveys are merged to create the following plots.

Table 1. Definition of the FoR and the measurement standard deviations σ (Radar: values at $\rho_r = 750$ km).

Size FoR, Radar	$60° \times 20°$
Angles (Radar), σ	$0.17°$
Range, σ	20 m
Rate, σ	20 $\frac{\text{m}}{\text{s}}$
Angles (Optical), σ	1”

For the optical measurements, the tracklet length is 90 s with a measurement each 15 s which is consistent with real measurements of HEO objects at the AIUB observatory in Zimmerwald. In case of the radar tracklets, their length depends on the dwell time in the Field of Regard (FoR), which can be up to two minutes and is approx. 40 s on average. These tracklets are used for the radar-optical case whereas the radar-only case employs 40 s tracklets without FoR to increase the number of detections and true correlations.

3.1. Mahalanobis Distance

Concerning the evaluation of the correlation experiments, one additional filter is introduced. As given in Equation 1, the radar attributable does not contain an information on the angular direction of motion which leads to an increased number of false positives. This is solved by checking if the azimuth residuals of the measured tracklets derived from the computed orbit have a linear trend instead of random variations and thus the orbit does not match the tracklet. This is performed via a Student’s t-test, similar to [4]. All results given in the following include this filtering.

The distributions of the Mahalanobis distances are plotted containing the true positives (TP), which are the correctly identified correlations of two tracklets from the same object. The other two cases, namely the false positives (FP), which are the wrongly identified correlations of two tracklets from different objects, and the true positives with a wrong orbit (WO), which means that the two tracklets belong together but the orbit to connect them has the wrong number of revolutions thus a large error in the semi-major axis, are not plotted. For all cases there are less than 5%-10% false positives after the additional azimuth filter.

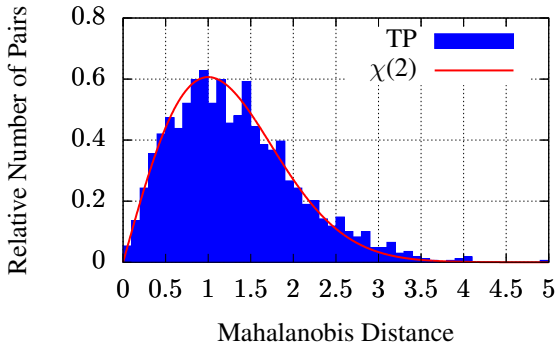

Figure 3. Distribution of the true positives’ Mahalanobis distances for the radar-only case.

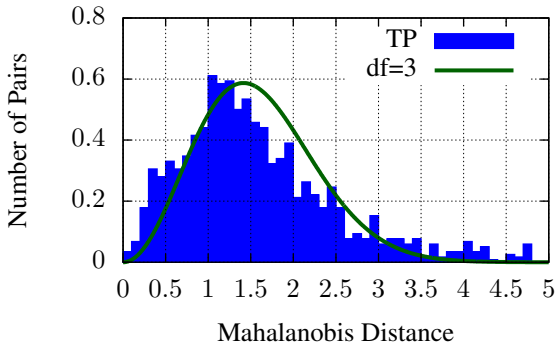

Figure 4. Distribution of the true positives’ Mahalanobis distances for the radar-optical case.

The distributions of the radar-only case in Figure 3 and

of the radar-optical case in Figure 4 are shown as relative numbers to compare them to the theoretically expected χ-distribution of the Mahalanobis distances depending on the degrees of freedom which is equal to the number of elements in the discriminator. Thus, the radar-only case has two degrees of freedom and the radar-optical case has three. As one can see, the radar-only case matches the expected χ-distribution very well, whereas the radar-optical one is slightly shifted to lower Mahalanobis distances but still exhibits a clear peak in the expected region.

3.2. Discriminator

This section shall analyse the influences of the different elements in the radar-optical discriminator to test whether the different physical measurement types have any specific influence. The following plots are also considering only true positives. Firstly, the range-rate discriminators are compared between the cases for radar-only and the radar-optical in Figure 5. Although the plot is two-dimensional, the range-rate discriminator for the radar-optical case is only one-dimensional and thus plotted along the x-axis. It is clear that the range-rate discriminators are similar in magnitude for both cases, which is also consistent with the assumed measurement noise. Additionally, it shall be noted that the two-dimensional distribution of discriminators for the radar-only case is consistent with a normal distribution, showing no biases or preferences to any direction, which implies that both range-rates have similar distributions of their differences in the discriminator. This is consistent with the orbit determination method, because it does not prefer one of the two positions and thus the discriminators should be distributed evenly. The same is true for the radar-optical case as the majority of the points are close to zero.

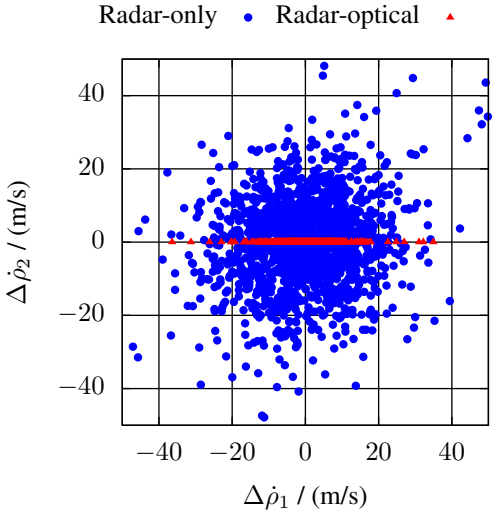

Figure 5. Distribution of the differences of the range-rate discriminators comparing the radar-only and radar-optical case.

Additionally, for the radar-optical case the discriminators in the optical part are compared in Figure 6. Also here, the discriminators are evenly distributed between the two angular rates within the same order of magnitude.

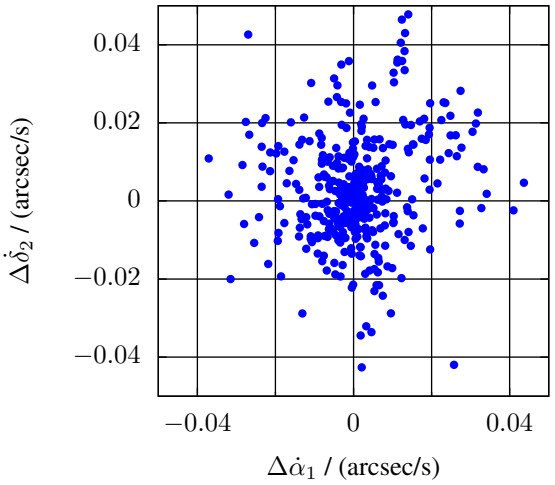

Figure 6. Distribution of the differences of the angular rates discriminators for the radar-optical case.

In order to analyse the influence of the discriminator in the radar-optical case in more detail, the covariance matrix $C_{m,c}$, thus also the Mahalanobis distance, is separated into the different elements of the discriminator and the uncertainties are split in their two contributing parts. This is achieved by assuming a diagonal correlation matrix without cross-correlations between the different discriminators, which is not fully achieved but can be used as an approximation. The overall covariance matrix $C_{m,c}$ of the discriminators is the sum of the measurement and computed orbit covariance as explained earlier:

$$C_{m,c} = \begin{bmatrix} \sigma^2_{\dot{\rho}_r,m} + \sigma^2_{\dot{\rho}_r,c} & 0 & 0 \\ 0 & \sigma^2_{\dot{\alpha},m} + \sigma^2_{\dot{\alpha},c} & 0 \\ 0 & 0 & \sigma^2_{\dot{\delta},m} + \sigma^2_{\dot{\delta},c} \end{bmatrix} \quad (4)$$

In combination with Equation 3 this leads to the following simplification for the calculation of the Mahalanobis distance:

$$M_{d,total} = \sqrt{M^2_{d,\dot{\rho}_r} + M^2_{d,\dot{\alpha}} + M^2_{d,\dot{\delta}}}\,. \quad (5)$$

The Mahalanobis distance for one discriminator x is calculated as:

$$M^2_{d,x} = \frac{\Delta x^2}{\sigma^2_{x,m} + \sigma^2_{x,c}} \quad (6)$$

With some algebraic transformations, this can be generalised to:

$$\frac{1}{M^2_{d,x}} = \frac{1}{M^2_{d,x,m}} + \frac{1}{M^2_{d,x,c}}\,, \quad (7)$$

with $M_{d,x,m}$ and $M_{d,x,c}$ as the Mahalanobis distances only due the measurement or orbit computation:

$$M^2_{d,x,m/c} = \frac{\Delta x^2}{\sigma^2_{x,m/c}} \,. \tag{8}$$

These relations are used in the following for further analyses.

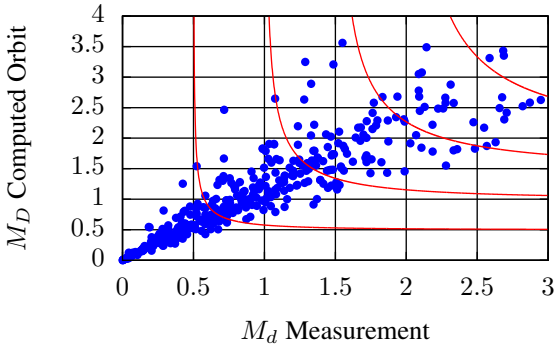

Figure 7. Contributions of the measurement and orbit uncertainties to the Mahalanobis distance at the radar measurement in the radar-optical case. Lines of constant combined Mahalanobis distance are added for $M_d = \{0.5, 1.0, 1.5, 2.0\}$.

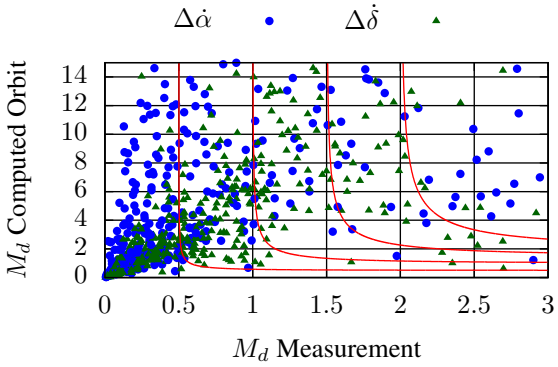

Figure 8. Contributions of the measurement and orbit uncertainties to the Mahalanobis distance at the optical measurement in the radar-optical case. Lines of constant combined Mahalanobis distance are added for $M_d = \{0.5, 1.0, 1.5, 2.0\}$.

Figure 7 depicts the range-rate discriminator split in its components, i.e. the measurement and orbit uncertainty. Lines of constant combined Mahalanobis distance are added to the plot according to Equation 7. It is visible that both components contribute approx. equally to the total Mahalanobis distance of the radar measurement. In contrast to that, Figure 8 compares the same values for the angular rates. In this case, the Mahalanobis distance due to the orbit is larger than the one due to the measurement. The lines of constant total Mahalanobis distance are predominantly acting as vertical straight lines, thus the total Mahalanobis distance is dominated by the measurement, see Equation 7. Effectively this means that $\sigma_c^2 \ll \sigma_m^2$, yielding $M^2_{d,c} \gg M^2_{d,m}$. The uncertainty due to the orbit computation is smaller than the one due to the measurement and contributes less to the total uncertainty when they are added.

Finally the influence of the different discriminators is compared according to Equation 5. Also here the lines of constant Mahalanobis distance are added which form an arc of a circle. Figure 9 compares the two optical discriminators, i.e. the angular rates. It is visible that considering the entire population both parts contribute equally to the total optical Mahalanobis distance.

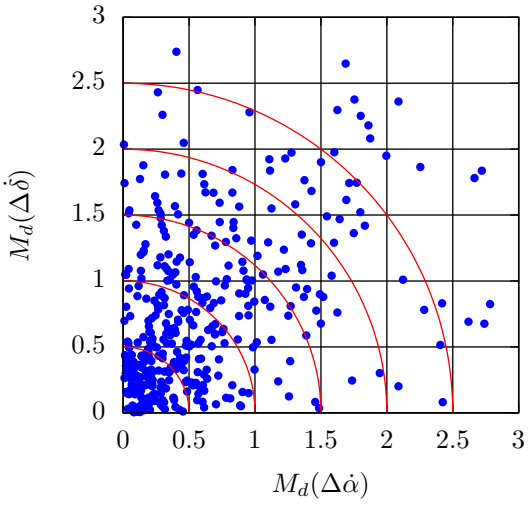

Figure 9. Contributions of the optical measurements to the total Mahalanobis distance in the radar-optical case. Lines of constant combined Mahalanobis distance are added for $M_d = \{0.5, 1.0, 1.5, 2.0, 2.5\}$.

The comparison between the radar-discriminator and the two optical discriminators is shown in Figure 10. Also here, it is visible that both measurement types contribute equally to the total Mahalanobis distance. Combining this information with the one derived from Figure 9, it is concluded that all three discriminators contribute equally to the total Mahalanobis distance.

3.3. Orbits

In Figure 11, the correlation results are compared with regard to the standard deviations for the estimation of the orbital elements semi-major axis a, eccentricity e, inclination i, right ascension of the ascending node Ω and argument of perigee ω, which are derived from their respective ground truth. It can be seen that the radar-optical measurements have better results than radar-only in all cases. Especially the location of the perigee and the estimation of the orbital plane is significantly better.

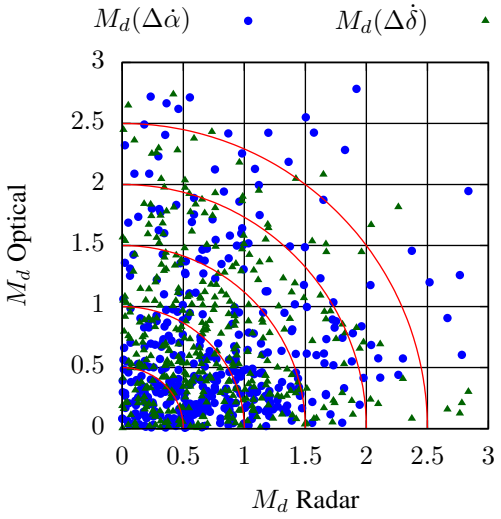

Figure 10. Contributions of the radar and optical measurements to the total Mahalanobis distance in the radar-optical case. Lines of constant combined Mahalanobis distance are added for $M_d = \{0.5, 1.0, 1.5, 2.0, 2.5\}$.

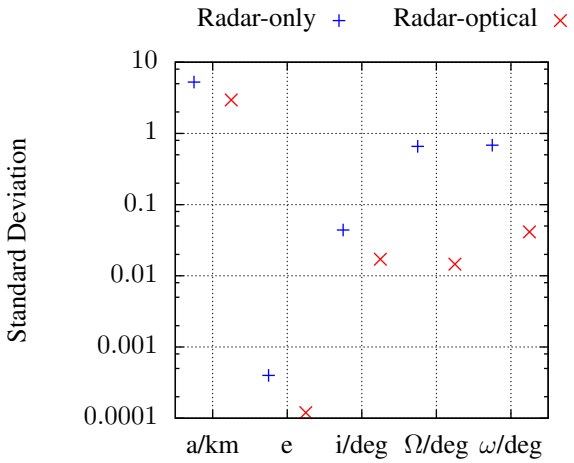

Figure 11. Comparison between the radar-only and radar-optical case for the standard deviations of the estimation errors of the orbital elements when compared to the ground truth.

4. DISCUSSION

The results presented in the previous section shall be further discussed and explained in the following. It was seen that while the radar-only case matches its theoretically expected χ-distribution very well, the one of the radar-optical case is slightly shifted towards smaller Mahalanobis distances. Possible explanations for this mismatch are e.g. the observation geometry for specific simulations, the estimated uncertainties from the least squares fit of the attributable or the linear transformation of the covariance matrix.

Concerning the details of the radar-optical correlation, one could see that the discriminators are all evenly distributed and their separated Mahalanobis distances are of similar magnitude. Thus, it can be concluded that neither of the discriminators is dominating the uncertainties and the method considers all in a similar way. It was also shown that the Mahalanobis distance of the angular rates is mainly dominated by the measurement uncertainty compared to the uncertainty of the computed orbit. This implies that the angular rates are rather robust against the noise in the parameters used for the orbit estimation, at least when compared to the measurement noise. To conclude this part, it is clear that neither of the uncertainties can be ignored to reduce the computational burden of the correlation process, because all contribute equally to the result even with different physical measurement types.

Considering the orbits, the main improvement of the radar-optical case is due to the better coverage of the orbit. The radar measurements are always close to the perigee, while the optical telescopes can add measurements close to apogee. This improves especially the estimation of the orbital plane and the shape of the ellipse as the angle between the two radius vectors used in the orbit determination increases. Concerning the semi-major axis, it was also estimated more precisely in the radar-optical case for a large data sample, but if the radar and optical measurements are close together, i.e. during the same revolution within a few hours, the estimation of the semi-major axis becomes significantly worse.

Finally, this approach also suffers from a degradation if the measurements are close to be on exactly opposite sides of the orbit, thus roughly 180° apart. In this case, problems may arise due to the rotations during the J_2-correction because the definition of the orbital plane is very sensitive to small changes in this region.

5. CONCLUSION

This paper proposed a method for the fusion of radar and optical measurements during the correlation and initial orbit determination process of space surveillance measurements. It was shown that the method works for samples of simulated survey measurements using different

scenarios. In general, this also leads to a better orbit quality than for the radar-only case, because the measurements cover a larger part of the orbit. One challenge of applying this to practical space surveillance is that the population of objects which can be observed at the perigee by a radar and at night-time at apogee by a telescope is very limited for single stations. Thus, this observation fusion method is probably most effective in multi-station networks which can reliably observe a majority of the relevant near-Earth regions.

ACKNOWLEDGMENTS

The author is supported by the European Space Agency through the Networking/Partnering Initiative.

REFERENCES

1. Braun, V., Lemmens, S., Reihs, B., et al., (2017). Analysis of Breakup Events. *Proc. 7th European Conference on Space Debris*, Darmstadt, Germany.
2. DeMars, K., Jah, M., (2013). Probabilistic initial orbit determination using gaussian mixture models. *Journal of Guidance, Control, and Dynamics*, **36**(5), 1324-1335.
3. Escobal, P., (1976). *Methods of orbit determination*, R.E. Krieger Pub. Co.
4. Fujimoto, K., Scheeres, D., Herzog, J., Schildknecht, T., (2014). Association of optical tracklets from a geosynchronous belt survey via the direct Bayesian admissible region approach. *Advances in space research*, **53**(2), 295–308.
5. Gronchi, G., Farnocchia, D., Dimare, L., (2011). Orbit determination with the two-body integrals. II. *Celestial Mechanics and Dynamical Astronomy*, **110**(3), 257-270.
6. Ma, H., Ba, G., Cioci, D., Gronchi, G., (2018). Preliminary orbits with line-of-sight correction for LEO satellites observed with radar. *Celestial Mechanics and Dynamical Astronomy*, **130**(10), 70.
7. Mahalanobis, P., (1936). On the generalised distance in statistics. *Proceedings of the National Institute of Science of India*, **2**(1), 49-55.
8. McKnight, D., Speaks, S., Macdonald, J., Ebright, K., (2018). Assessing Potential for Cross-Contaminating Breakup Events from LEO to MEO/GEO. *69th International Astronautical Congress*, Bremen, Germany.
9. Milani, A., Sansaturio, M., Chesley, S., (2001). The asteroid identification problem IV: Attributions. *Icarus*, **151**(2), 150-159.
10. Orekit, (2018). A space dynamics library. https://www.orekit.org/.
11. Reihs, B., Vananti, A., Schildknecht, T., (2018). Comparison of new methods for the correlation of short radar tracklets. *69th International Astronautical Congress*, Bremen, Germany.
12. Siminski, J., Montenbruck, O., Fiedler, H., Schildknecht, T., (2014). Short-arc tracklet association for geostationary objects. *Advances in space research*, **53**(8), 1184–1194.
13. Space-Track, (2018). https://www.space-track.org/.
14. Vananti, A., Schildknecht, T., Siminski, J., et al., (2017). Tracklet-tracklet correlation method for radar and angle observations. *Proc. 7th European Conference on Space Debris*, Darmstadt, Germany.